Scattering from oriented objects analysed by the anisotropic Guinier–Porod model

Tian, Bei; Heringa, Jouke R.; Bouwman, Wim G.

DOI
10.1016/j.foostr.2021.100221

Publication date
2021

Document Version
Final published version

Published in
Food Structure

Food Structure 30 (2021) 100221

Contents lists available at ScienceDirect

Food Structure

journal homepage: www.elsevier.com/locate/foostr

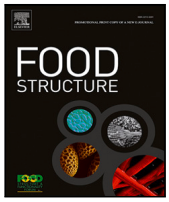

Scattering from oriented objects analysed by the anisotropic Guinier–Porod model

Bei Tian, Jouke R. Heringa, Wim G. Bouwman *

Department of Radiation Science and Technology, Faculty of Applied Science, Delft University of Technology, Mekelweg 15, 2629JB Delft, The Netherlands

ARTICLE INFO

Keywords:
Guinier–Porod model
Anisotropy
Small angle scattering
Oriented objects
Fibrous protein gel

ABSTRACT

Small angle scattering is frequently applied to study the anisotropy in complex soft matter systems. One emerging application is to probe the multi-scale structure in food matrices; while few models are available to describe the anisotropic scattering pattern in a quantitative, yet simple manner. For this purpose, anisotropy is introduced to the Guinier–Porod model to study the scattering from non-spherical objects with a preferred orientation. This generalised anisotropic Guinier–Porod model can be adapted to approximate the sector scattering from both cylinders and ellipsoids (both prolate and oblate). In practice, it is applied to describe the anisotropic scattering from fibres in a meat analogue made of calcium caseinate. A good agreement is found between fitted dimensions of the fibres and those observed from the microscopy image. The effect of orientation distribution on the shape and intensity of the scattering pattern is further discussed and three means to obtain the orientation distribution of the symmetry axis are proposed. Given the model is straightforward and the fitting remains phenomenological, it provides a novel approach to extract information from complex food systems.

1. Introduction

Many samples display anisotropy in their two-dimensional (2D) small-angle scattering (SAS) patterns. Anisotropy can be introduced through means such as compression, particle alignment under shear flow or orientation in a magnetic field (Gazeau et al., 2002; Maranzano & Wagner, 2002; Weigandt, Porcar, & Pozzo, 2011).

There are in general three approaches to extract information from anisotropic scattering data. When a priori knowledge on the shape of the scattering object is available, the first approach is to fit the data with a shape-dependent model. For instance, the form factor of an oriented cylinder has been applied to study the scattering patterns of gel networks containing fibrins (Weigandt et al., 2011) or rod-like fibrils (Maki et al., 2011; Yong et al., 2002); it has also been used to describe the local structure of branched micelles or wormlike micelles (Förster, Konrad, & Lindner, 2005; Vogtt, Beaucage, Weaver, & Jiang, 2015; Won, Davis, & Bates, 1999; Worcester, Michalski, & Katz, 1986).

When the shape of the object is less well defined or unknown, the scattering intensity can be described using a model without a specific geometry, which will be categorised as a shape-independent model. The Ornstein–Zernike function was used to study the correlation length of uniaxially deformed polymer networks in the Tetra-PEG gel (Matsunaga et al., 2011) and clay nanocomposite gels (Miyazaki, Karino, Endo, Haraguchi, & Shibayama, 2006); a sum of squared-Lorentz function and the scattering from randomly oriented thin rods were applied to study stretched slide-ring gels (Karino et al., 2005); the unified power law is introduced to study systems with multiple structural levels (Beaucage, 1995, 1996; Beaucage, Ulibarri, Black, & Schaefer, 1995; Ratnaweera et al., 2015); and the Debye function was applied to study the radius of gyration of the Shish nuclei under extension flow (Yang et al., 2016).

A third and simpler approach is to parametrise only changes in the peak position and slope in the scattering pattern, without performing a global fit. This was used in the analysis of sector intensities of a visco-elastic polymer-clay solution at different shear rates (Schmidt, Nakatani, Butler, & Han, 2002), as well as the crystallisation behaviour of poly(lactic-acid) polymers during annealing (Mahendrasingam et al., 2005).

Different challenges were encountered when using the above-mentioned three approaches to quantify the change of fibre sizes as a function of processing parameters. For the shape-dependent model, it will require a broad size distribution to smoothen sharp interference peaks coming from a form factor; for a shape-independent model, the interpretation of the physical meaning of fitted parameters will be limited since they are not attributed to a specific shape; and an overall description of the fibre-containing system will be missing for the third

* Corresponding author.
E-mail address: w.g.bouwman@tudelft.nl (W.G. Bouwman).

https://doi.org/10.1016/j.foostr.2021.100221
Received 18 December 2020; Received in revised form 2 August 2021; Accepted 21 August 2021
Available online 9 September 2021

approach in absence of a global fit. Apart from studies conducted in polymer science, SAS, in recent years, has also been applied to food or bio-macromolecules. For instance, small angle neutron scattering was recently applied to study the anisotropic scattering from meat analogues which contain pronounced fibrous structures (Tian et al., 2020). Since the compositions or shapes of food and bio-macromolecules are often less well defined or highly polydisperse, it has posed even more challenges to the analysis of the rather featureless anisotropic scattering patterns. As a result, new models are needed to provide quantitative descriptions for the scattering from meat analogues and many other food systems with complicated structures.

We present a new anisotropic Guinier–Porod model to describe the scattering pattern of objects with a preferred orientation. The model is first presented in its general form, then applied to approximate the sector intensities of cylinders and ellipsoids. To demonstrate the practicality of this model, it is used to fit the anisotropic scattering data from oriented fibres in the meat analogue produced at one processing parameter. For the complete fitting of this model at other processing parameters, the reader is referred to the paper (Tian et al., 2020). The effect due to the orientation distribution of the symmetry axis on the scattering pattern is further discussed and three means to obtain the distribution of orientation are proposed.

2. The generalised anisotropic Guinier–Porod model

A form factor $F_{\mathrm{aGP}}(Q,\alpha)$ in the generalised anisotropic Guinier–Porod model has the following form:

$$F_{\mathrm{aGP}}(Q,\alpha)=\begin{cases} e^{-\frac{d}{2}\left(\frac{Q}{Q_0(\alpha)}\right)^2} & Q\le Q_0(\alpha) \\ \left(\dfrac{Q_0(\alpha)}{Q\cdot\sqrt{e}}\right)^d & Q\ge Q_0(\alpha), \end{cases} \tag{1}$$

where Q is the scattering vector, α is the angle between the orientation direction of the object and Q, which can vary from 0 to π, d is the exponent and $Q_0(\alpha)$ is the transition point, determined by the dimensions of the object and α. Similar to the original Guinier–Porod model (Hammouda, 2010), when $Q_0(\alpha)$ is averaged over the full angle, the radius of gyration R_g of the object can be obtained, following the relation that $Q_0=\frac{1}{R_g}\sqrt{\frac{3d}{2}}$. The interpretation of the exponent also holds, so that $d=-4$ at high-Q suggests a smooth interface from large particles. Moreover, this generalised form satisfies requirements that both the Guinier and Porod terms as well as their derivatives are continuous at a given $Q_0(\alpha)$.

The construction of the generalised anisotropic Guinier Porod model enables flexibility in describing the scattering pattern of a variety of objects. In the following sections, applications of the model are given to objects in dilute systems with well defined shapes and to a real, jammed system with less defined shape.

3. Applications of the model

3.1. Approximating the sector intensity of oriented cylinders

The form factor of an oriented cylinder is given by Fournet (1951), Guinier, Fournet, and Walker (1955):

$$P_{\mathrm{cylinder}}(Q,\alpha)=\left[\frac{\sin(Q\cdot\cos\alpha\cdot\frac{L}{2})}{Q\cdot\cos\alpha\cdot\frac{L}{2}}\cdot\frac{2J_1(Q\cdot\sin\alpha\cdot\frac{D}{2})}{Q\cdot\sin\alpha\cdot\frac{D}{2}}\right]^2 \tag{2}$$

where L and D are the length and diameter of the cylinder respectively, J_1 is the Bessel function of the first kind. $P_{\mathrm{cylinder}}(Q,\alpha)$ can be approximated by the product of two form factors defined in Eq. (1):

$$P_{\mathrm{cylinder}}(Q,\alpha)\approx P_{\mathrm{aGP,\ cyl}}(Q,\alpha)=F_l(Q,\alpha)\cdot F_r(Q,\alpha) \tag{3}$$

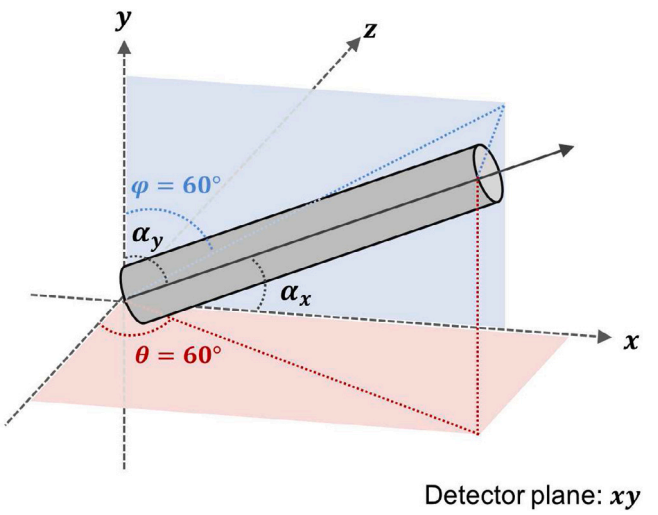

Fig. 1. A schematic representation of the orientation of a cylinder in the Cartesian coordinate. The cylinder is placed as such that the angle (φ) between the projection of the cylinder (onto the detector plane) and the y-axis equals 60° and the angle (θ) between the projection (onto the xz plane) and z-axis also equals 60°. From Eq. (6), one can calculate that when the direction of Q is parallel to the x-axis, the angle α_x between Q and the orientation axis equals 39°, while when the direction of Q is parallel to the y-axis, the angle $\alpha_y=63°$.

where

$$F_l(Q,\alpha)=\begin{cases} e^{-\frac{d_l}{2}\left(\frac{Q}{Q_l(\alpha)}\right)^2} & Q\le Q_l(\alpha) \\ \left(\dfrac{Q_l(\alpha)}{Q\cdot\sqrt{e}}\right)^{d_l} & Q\ge Q_l(\alpha) \end{cases} \tag{4}$$

$$F_r(Q,\alpha)=\begin{cases} e^{-\frac{d_r}{2}\left(\frac{Q}{Q_r(\alpha)}\right)^2} & Q\le Q_r(\alpha) \\ \left(\dfrac{Q_r(\alpha)}{Q\cdot\sqrt{e}}\right)^{d_r} & Q\ge Q_r(\alpha) \end{cases} \tag{5}$$

Eqs. (4) and (5) show that two transition points $Q_l(\alpha)$ and $Q_r(\alpha)$ are needed to describe the scattering function, where $Q_l(\alpha)=\frac{\sqrt{6d_l}}{L\cdot\cos\alpha}$ and $Q_r(\alpha)=\frac{\sqrt{6d_r}}{D\cdot\sin\alpha}$, d_l and d_r are the exponents, where $d_l=2$ and $d_r=3$. In essence, $F_l(Q,\alpha)$ approximates the Guinier and Porod regions of $\left[\frac{\sin(Q\cdot\cos\alpha\cdot\frac{L}{2})}{Q\cdot\cos\alpha\cdot\frac{L}{2}}\right]^2$ and $F_r(Q,\alpha)$ describes the scattering features of $\left[\frac{2J_1(Q\cdot\sin\alpha\cdot\frac{D}{2})}{Q\cdot\sin\alpha\cdot\frac{D}{2}}\right]^2$ in the original form factor.

Two perpendicular sector intensities are usually plotted to show the anisotropy in the scattering pattern. The horizontal intensity is the intensity along the x-axis, in which case the direction of Q is parallel to the x-axis and the angle between Q (or the x-axis) and the orientation axis of the cylinder is denoted as α_x. Similarly, the vertical intensity can be obtained in case when the direction of Q is parallel to the y-axis, and α_y is the angle between Q (or the y-axis) and the axis of the cylinder. α_x and α_y can be calculated knowing the reference orientation of the object with respect to the detector (Fournet, 1951).

$$\begin{aligned} \alpha_x &= \arctan\sqrt{(\cot\theta)^2+(\cot\varphi)^2} \\ \alpha_y &= \arctan\left(\frac{\tan\varphi}{\sin\theta}\right) \end{aligned} \tag{6}$$

As illustrated in Fig. 1, φ is the angle between the projection of the orientation axis onto the detector plane and the y-axis, θ is the

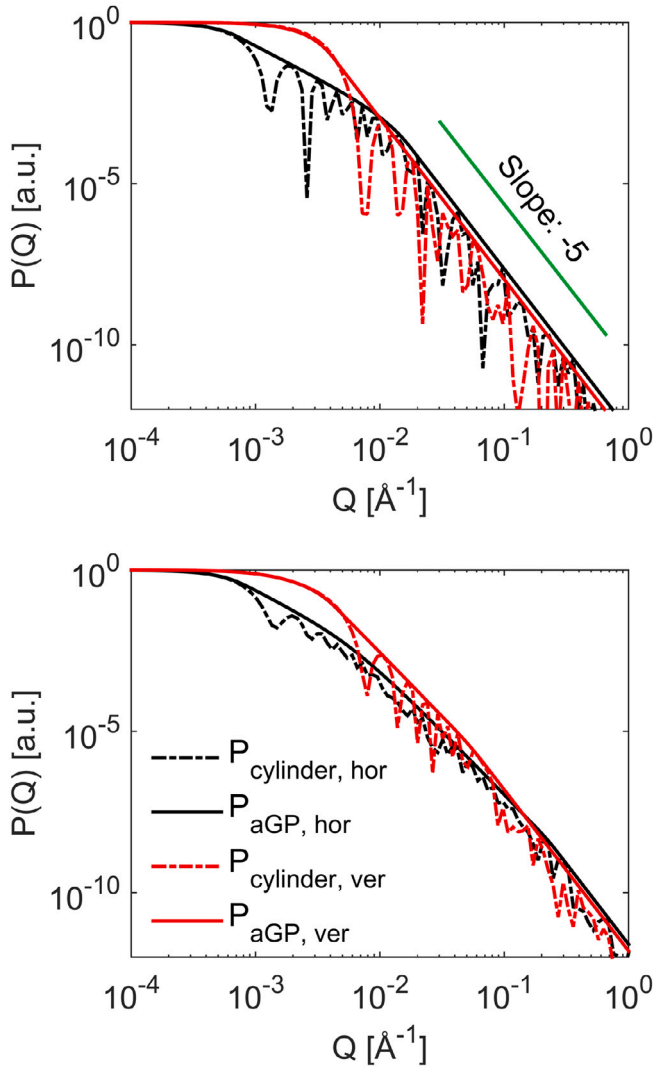

Fig. 2. Horizontal (black) and vertical (red) intensities calculated from the form factor of oriented cylinders (dot dashed lines) and the corresponding anisotropic Guinier–Porod model (solid lines). The cylinder is oriented as such that $\alpha_x = 14°$ and $\alpha_y = 80°$. The diameter of the cylinder is 100 nm, and the length is 500 nm. Top: axes of cylinders are perfectly oriented; Bottom: a Gaussian distribution of the orientation of the axis is included, with a standard deviation of 30°. (For interpretation of the references to colour in this figure legend, the reader is referred to the web version of this article.)

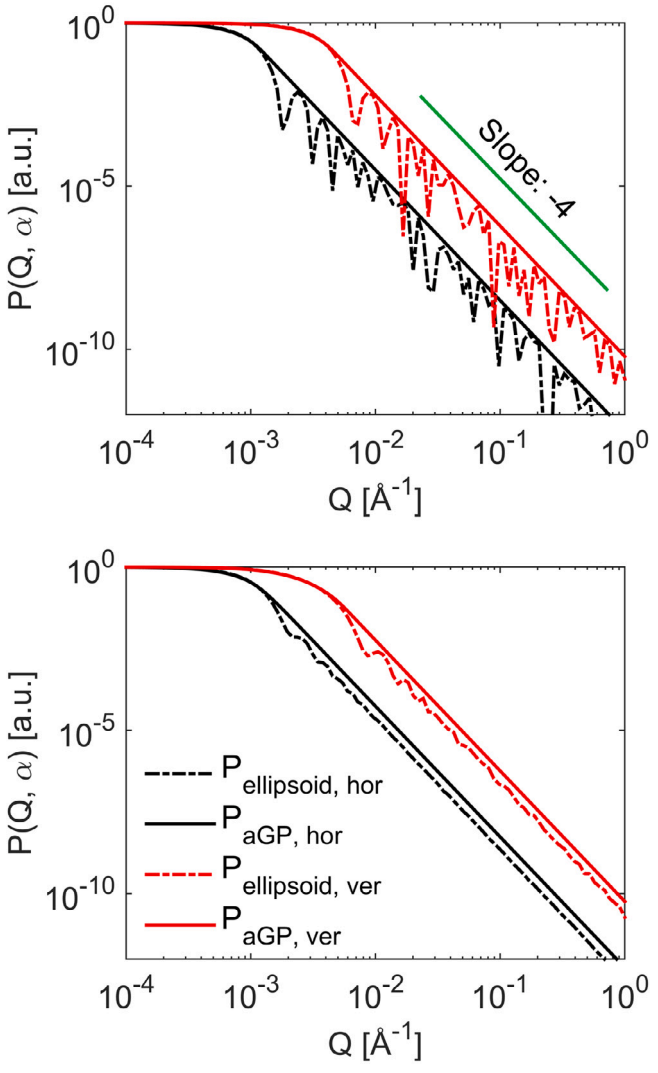

Fig. 3. Horizontal (black) and vertical (red) intensities calculated from the form factor of oriented ellipsoids (dot dashed lines) and the corresponding anisotropic Guinier–Porod model (solid lines). The ellipsoid is placed at $\alpha_x = 14°$ and $\alpha_y = 80°$. The equatorial radius of the ellipsoid is 50 nm, and the polar radius is 250 nm. Top: polar axes of ellipsoids are perfectly oriented; Bottom: a Gaussian distribution of the orientation of the axis is included, with a standard deviation of 30°. (For interpretation of the references to colour in this figure legend, the reader is referred to the web version of this article.)

angle between the projection of the orientation axis onto the xz-plane and the z-axis. Thus, the scattering in the horizontal direction can be calculated as $P_{\text{aGP, cyl, hor}} = F_l(Q,\alpha_x) \cdot F_r(Q,\alpha_x)$, and $P_{\text{aGP, cyl, ver}} = F_l(Q,\alpha_y) \cdot F_r(Q,\alpha_y)$ in the vertical direction. Sector intensities of both perfectly oriented cylinders and cylinders with an orientation distribution, as well as their corresponding anisotropic Guinier–Porod models are plotted in Fig. 2. Together they show that the model captures very well the slopes and transition points of cylinders with or without orientation distribution.

3.2. Approximating the scattering intensity of oriented ellipsoids

The form factor of an oriented ellipsoid is given by Feigin, Svergun, et al. (1987):

$$P_{\text{ellipsoid}}(Q,\alpha) = \left[\frac{3(\sin(Qr_e(\alpha)) - Qr_e(\alpha)\cdot\cos(Qr_e(\alpha)))}{(Qr_e(\alpha))^3}\right]^2$$
$$r_e(\alpha) = \sqrt{(R_e\cdot\sin\alpha)^2 + (R_p\cdot\cos\alpha)^2} \tag{7}$$

where R_e is the equatorial radius and R_p is the polar radius. It can be approximated by the anisotropic Guinier Porod model as:

$$P_{\text{ellipsoid}}(Q,\alpha) \approx P_{\text{aGP, ell}}(Q,\alpha) = F_e(Q,\alpha)^2 \tag{8}$$

where

$$F_e(Q,\alpha) = \begin{cases} e^{-\frac{d_e}{2}\left(\frac{Q}{Q_e(\alpha)}\right)^2} & Q \le Q_e(\alpha) \\ \left(\dfrac{Q_e(\alpha)}{Q\cdot\sqrt{e}}\right)^{d_e} & Q \ge Q_e(\alpha) \end{cases} \tag{9}$$

Unlike for the cylinder, the scattering function of the ellipsoid (applicable for both prolate and oblate) is defined by only one transition point Q_e, where $Q_e = 3/r_e(\alpha)$. The exponent d_e equals 2 for a smooth surface. The horizontal and vertical sector intensity of oriented ellipsoids and their corresponding anisotropic Guinier–Porod models are presented in Fig. 3.

Even though the sector scattering patterns for perfectly oriented objects display a rapidly oscillating behaviour at high Q (top figures in Figs. 2 and 3), this is rarely measured in real experiments due to finite Q resolution, non-sharp particle boundaries and background noise, etc. In this sense, the Porod regime in the anisotropic model is sufficient to give a satisfactory description of the system.

3.3. Approximating the scattering from a fibrous protein gel

Pronounced fibres are formed in a calcium caseinate gel after mild shearing and heating (Manski, van der Goot, & Boom, 2007). Microscopy images from previous works (Manski et al., 2007; Wang, Tian, Boom, & van der Goot, 2019) have shown that these cylinder-like fibres are composed of sphere-like particles aligned along the shear flow direction. To study the size and orientation of the structure, one fibrous gel sample, with a thickness of 1.5 mm, prepared by Dr. Zhaojun Wang, was measured at room temperature using the BILBY instrument at the OPAL reactor, Australian Nuclear Science and Technology Organisation (ANSTO) (Tian et al., 2020). A combined Guinier–Porod model is used to model the sector intensity:

$$I(Q) = G_f \cdot F_l(Q,\alpha) \cdot F_r(Q,\alpha) + G_s \cdot F_s(Q) + \text{Background}. \tag{10}$$

In the above equation, $G_f \cdot F_l(Q,\alpha) \cdot F_r(Q,\alpha)$ describes the scattering intensity from the cylinder-like fibres at low Q, where $F_l(Q,\alpha)$ and $F_r(Q,\alpha)$ can be found in Eqs. (4) and (5). Given the fibrous gel contains 30% w/w protein, it is a jammed system. Yet, considering the model is phenomenological, no structure factor is involved, and G_f is purely an intensity factor. Its value will be in the same order of magnitude of the product of $\Delta\rho$ squared ϕ and V, which are the scattering length density contrast between the cylinders and the surrounding matrix, the volume fraction as well as the volume of the cylinder.

The isotropic scattering from the sphere-like particles at high Q is describe by $G_s \cdot F_s(Q)$, where:

$$F_s(Q) = \begin{cases} e^{\frac{-(Q\cdot R_g)^2}{3}} & Q \le Q_1 \\ e^{\frac{-(Q_1\cdot R_g)^2}{3}} \cdot \left(\frac{Q_1}{Q}\right)^{d_s} & Q \ge Q_1 \end{cases} \tag{11}$$

R_g is the radius of gyration of the sphere, d_s is the exponent that can vary between 1 and 3 (Beaucage, 1995), depending on the roughness of the surface. $Q_1 = \frac{1}{R_g}\sqrt{\frac{3d_s}{2}}$ (Hammouda, 2010). Similar to G_f, G_s is also a qualitative fitting parameter.

The fitting of two perpendicular sector intensities is conducted simultaneously using the SasView software (Doucet et al., 2017). Measured sector intensities and the combined Guinier–Porod model are presented in Fig. 4. Fitted parameters show that the fibre has a diameter of 64 ± 1 nm, a length of 437 ± 79 nm, and a R_g of 14.8 ± 0.1 nm. These numbers are in accordance with reported values obtained from microscopy images (Manski et al., 2007).

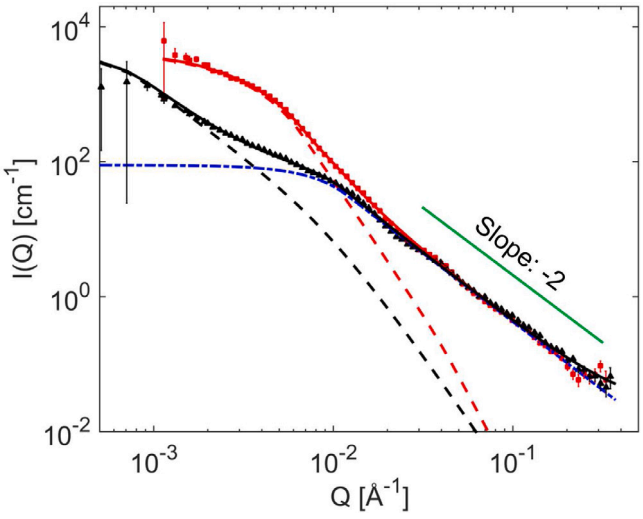

Fig. 4. Horizontal (black triangles) and vertical (red squares) intensities of the fibrous calcium caseinate gel modelled by the sum of (solid lines) the anisotropic and isotropic Guinier–Porod model. Anisotropic contributions from cylinder-like fibres are presented by the red dashed line in the vertical direction and by the black dashed line in the horizontal direction. The isotropic scattering from spheres is presented by the blue dot dashed line. The background is 0.02 ± 0.01 [cm^{-1}]. (For interpretation of the references to colour in this figure legend, the reader is referred to the web version of this article.)

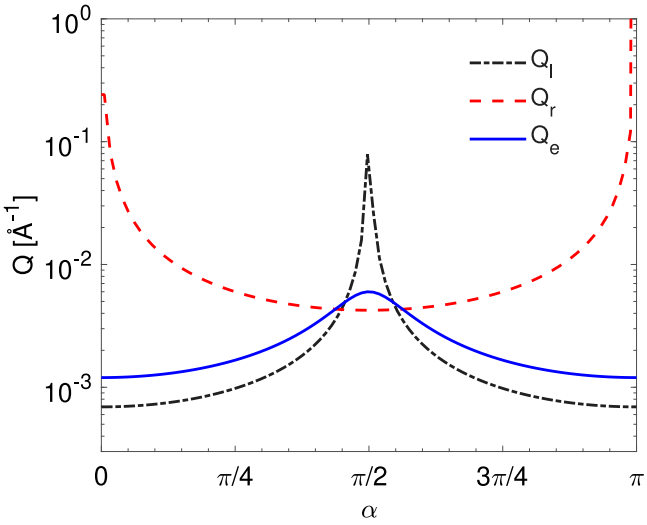

Fig. 5. Trends of transition points Q_l, Q_r of the cylinder (dot dashed line and dashed line) and Q_e of the ellipsoid (blue line) as a function of the angle α. The diameter of the cylinder is 100 nm and the length is 500 nm; the equatorial radius of the ellipsoid is 50 nm and the polar radius is 250 nm. (For interpretation of the references to colour in this figure legend, the reader is referred to the web version of this article.)

4. Discussion

It is common for oriented objects to have orientation distributions, thus, its influence on the scattering pattern will be discussed. Comparing the bottom figure in Fig. 2 to that in Fig. 3, it appears that orientation distribution has more impact on the shape of the scattering pattern of cylinders than ellipsoids. This is because the transition region of cylinders is determined together by Q_l and Q_r and they follow an opposite trend at varying angles α, as depicted in Fig. 5. As a result, when orientation distribution is included, the transition region will be defined by, instead of a single set of Q_l and Q_r, a series of Q_l-s or Q_r-s, which make the transition more gradual. Plus the opposite trend between Q_l and Q_r, the resulting transition region becomes even broader and smoother. While for ellipsoids, the transition region is determined only by the 'surface to centre distance', R_e, which follows a monotonic increase from 0-π/2 (Fig. 5). This will only lead to a slight broadening in the curvature of the transition region instead of a change of the total shape. The trend of R_e also hinted at the intensity difference between the model and the form factor of ellipsoids. Since every scattering pattern within the distribution follows a horizontal shift along the Q, the sharp interference peaks in the form factor will be averaged out after integration, which lead to a decrease of intensity in the Porod regime.

As for the fibrous protein gel, a Gaussian distribution with a standard deviation of 20° is included in α_x and α_y during fitting of the sector intensities. It is observed that fitted sizes of the cylinder are dependent on the standard deviation of the orientation distribution: the larger the

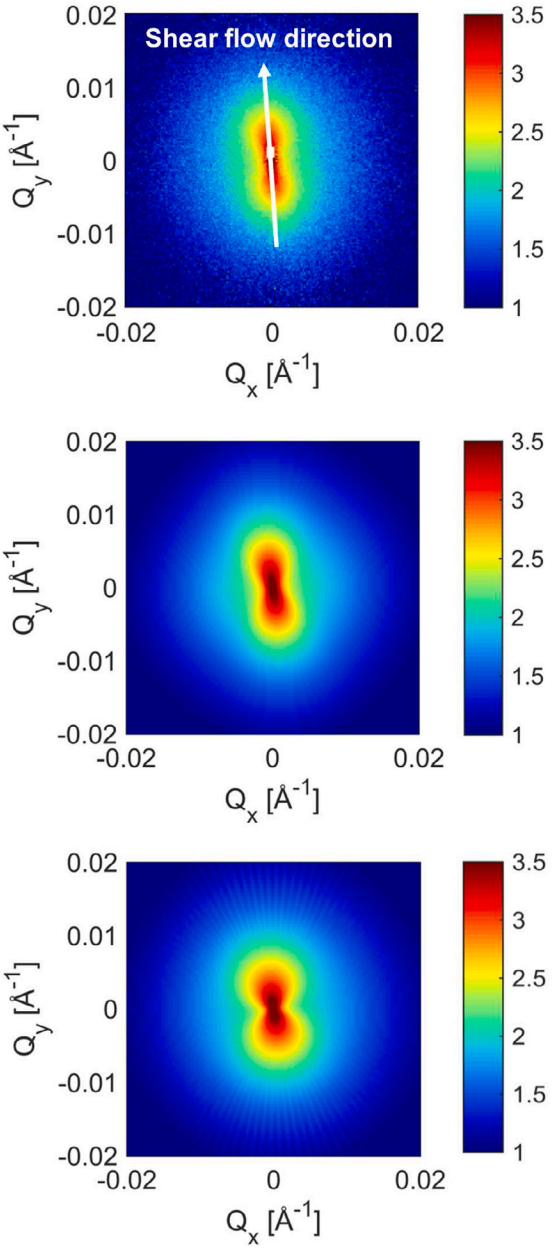

Fig. 6. Measured and calculated 2D scattering patterns of the fibrous calcium caseinate gel. The intensity uses a logarithmic scale. Top: measured 2D pattern of the sample; Middle: calculated scattering pattern with a fibre diameter of 64 nm, a length of 437 nm, and a standard deviation of 20° on a Gaussian orientation distribution; Bottom: calculated scattering pattern with a fibre diameter of 59 nm, a length of 824 nm, and a standard deviation of 30° on a Gaussian orientation distribution.

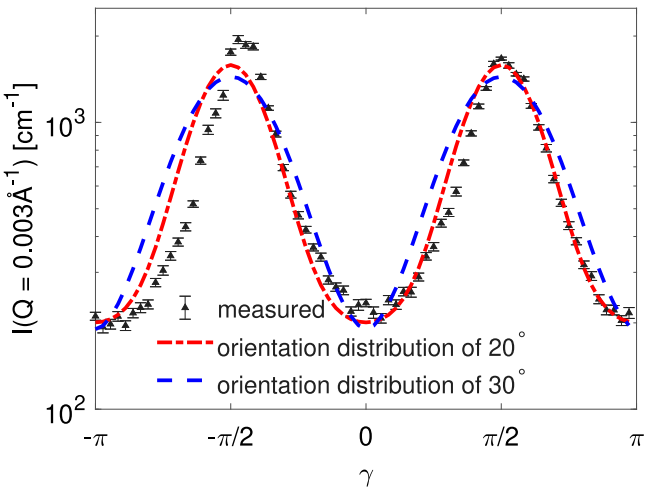

Fig. 7. Annular intensities at $Q = 0.003$ Å measured as a function of γ, which is the angle in the detector plane with respect to the x-axis. The black triangles are data measured from the fibrous calcium caseinate gel, the lines are calculated from the anisotropic Guinier–Porod model with a Gaussian orientation distribution of either 20° or 30°.

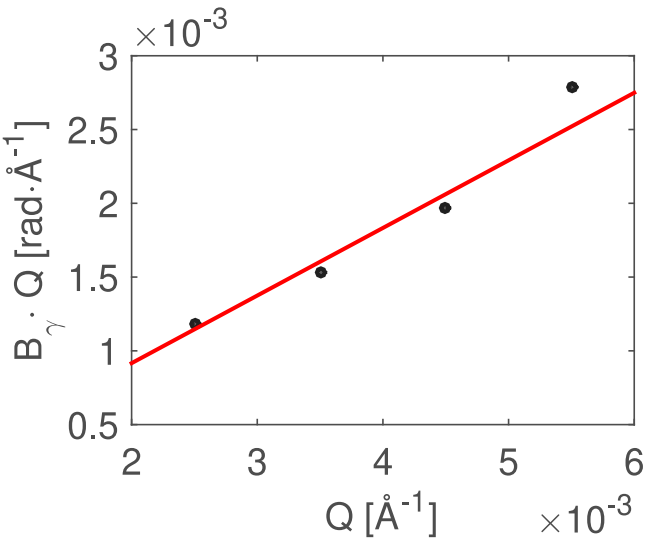

Fig. 8. The angular distribution B_γ multiplied by Q plotted as a function of Q. The red line is a linear fit of the data, it has a slope of 0.458 and intersects at 1.7×10^{-8} [rad · Å^{-1}]. (For interpretation of the references to colour in this figure legend, the reader is referred to the web version of this article.)

standard deviation, the higher the aspect ratio of the cylinder, while the quality of the fit remains similar. Thus, other methods are needed to ascertain the orientation distribution of the fibres, as it also indicates on the anisotropy of the system.

The first and most straightforward way is to compare calculated 2D scattering patterns with the measured one, as shown in Fig. 6. When the standard deviation of the orientation distribution is too large (30°), the scattering pattern will be overly smeared in the direction parallel to the shear flow (Fig. 6, bottom). The second way is to compare the distribution of the annular intensity at a given Q. Fig. 7 shows that the calculated annular intensity deviates more significantly from the measured one when the standard deviation of the orientation distribution is too large (30°). The third method is proposed by Ruland. et al. which has been applied to study the orientation distribution of many fibre-containing systems (An et al., 2016; Maurya et al., 2019; Perret & Ruland, 1969; Ruland, 1969). The angular intensity distribution at a certain Q is fitted with the Lorentzian function. The angular distribution B_γ is indicated by the half-width half maximum of the Lorentzian function. B_γ multiplied by Q is plotted against Q, as shown in Fig. 8. Given the linear relationship between $B_\gamma \cdot Q$ and Q, the orientation distribution can be extracted as the slope. In our case, it has an angle of 26°. Consistency between these three methods thus confirm that the fibres have an orientation distribution of ~20°.

Due to practical limitations, the anisotropic Guinier–Porod model is applied to only one real system. Yet, given its flexibility and simplicity, it is expected to extract information from other complex soft matter systems. When the geometry of the scattering object is known, the model can be directly adapted to describe the scattering pattern. For instance, the generalised anisotropic Guinier–Porod model in the case of ellipsoids can be used to describe oil droplets under shear or

compression; the cylindrical geometry can be used to characterise the dimension of tubes or cylindrical micelles. When the geometry is less certain, the model can be used to fit the data directly, given it has few parameters. However, the physical interpretation of the fitted results should be limited, because the construction of the model is based on the empirical approach by Hammouda (2010), instead of the more classical approaches by Beaucage (1995, 1996) or Debye (1947), thus, the fit remains phenomenological.

5. Conclusion

The anisotropic Guinier–Porod model is introduced as an empirical approach to describe the scattering from non-spherical objects with a preferred orientation. Depending on the a priori information, the model cannot only be adapted to approximate the scattering from objects in dilute systems with a certain shape, such as that of cylinders or ellipsoids, it can also be applied to study systems with less well defined shapes or structures, such as oriented fibres in a calcium caseinate gel. The dimensions of the fibres obtained from the fitted parameters are in good agreement with these observed from the microscopy image. It is further discovered that orientation distribution has more influence on the broadening of the transition region of the cylinder than on the ellipsoid. In summary, the flexibility and practicality offered by the anisotropic Guinier–Porod model makes it useful to extract information from real and complex systems, it also enables comparative studies of samples prepared at varying processing conditions.

Declaration of Competing Interest

The authors declare that they have no known competing financial interests or personal relationships that could have appeared to influence the work reported in this paper.

Acknowledgements

This work benefited from the use of the SasView application (Doucet et al., 2017) (http://www.sasview.org/), originally developed under NSF award DMR-0520547. SasView contains code developed with funding from the European Union's Horizon 2020 research and innovation programme under the SINE2020 project, grant agreement No 654000. We acknowledge beamtimes from the BILBY instrument from which the presented SANS data were obtained. Moreover, we would like to thank Dr. Stephen King for guidance on the usage of the SasView software, Dr. Steven Parnell for proofreading and constructive feedback on the content. This work is part of the research programme SSCANFoods (project number 13386), which is partly financed by the Netherlands Organisation for Scientific Research (NWO). A video presentation of this paper can be found at doi.org/10.5281/zenodo.5068028.

Appendix A. Supplementary data

Supplementary material related to this article can be found online at https://doi.org/10.1016/j.foostr.2021.100221.

References

An, M., Xu, H., Lv, Y., Gu, Q., Tian, F., & Wang, Z. (2016). An in situ small-angle X-ray scattering study of the structural effects of temperature and draw ratio of the hot-drawing process on ultra-high molecular weight polyethylene fibers. *RSC Advances*, *6*(56), 51125–51134.

Beaucage, G. (1995). Approximations leading to a unified exponential/power-law approach to small-angle scattering. *Journal of Applied Crystallography*, *28*(6), 717–728.

Beaucage, G. (1996). Small-angle scattering from polymeric mass fractals of arbitrary mass-fractal dimension. *Journal of Applied Crystallography*, *29*(2), 134–146.

Beaucage, G., Ulibarri, T., Black, E., & Schaefer, D. (1995). Multiple size scale structures in silica—siloxane composites studied by small-angle scattering. In *Hybrid organic–inorganic composites* (pp. 97–111). ACS Publications.

Debye, P. (1947). Molecular-weight determination by light scattering. *The Journal of Physical Chemistry*, *51*(1), 18–32.

Doucet, M., Cho, J., Alina, G., Bakker, J., Bouwman, W., Butler, P., et al. (2017). SasView Version 4.2.0. http://dx.doi.org/10.5281/zenodo.1412041.

Feigin, L., Svergun, D. I., et al. (1987). *Vol. 1, Structure analysis by small-angle X-ray and neutron scattering*. Springer.

Förster, S., Konrad, M., & Lindner, P. (2005). Shear thinning and orientational ordering of wormlike micelles. *Physical Review Letters*, *94*(1), Article 017803.

Fournet, G. (1951). Étude théorique et expérimentale de la diffusion des rayons X par les ensembles denses de particules. *Bulletin de Minéralogie*, *74*(1), 37–172.

Gazeau, F., Dubois, E., Bacri, J.-C., Boué, F., Cebers, A., & Perzynski, R. (2002). Anisotropy of the structure factor of magnetic fluids under a field probed by small-angle neutron scattering. *Physical Review E*, *65*(3), Article 031403.

Guinier, A., Fournet, G., & Walker, C. (1955). *Small-angle scattering of X-rays*. John Wiley & Sons, New-York.

Hammouda, B. (2010). A new Guinier–Porod model. *Journal of Applied Crystallography*, *43*(4), 716–719.

Karino, T., Okumura, Y., Zhao, C., Kataoka, T., Ito, K., & Shibayama, M. (2005). SANS studies on deformation mechanism of slide-ring gel. *Macromolecules*, *38*(14), 6161–6167.

Mahendrasingam, A., Blundell, D., Parton, M., Wright, A., Rasburn, J., Narayanan, T., et al. (2005). Time resolved study of oriented crystallisation of poly (lactic acid) during rapid tensile deformation. *Polymer*, *46*(16), 6009–6015.

Maki, Y., Ito, K., Hosoya, N., Yoneyama, C., Furusawa, K., Yamamoto, T., et al. (2011). Anisotropic structure of calcium-induced alginate gels by optical and small-angle X-ray scattering measurements. *Biomacromolecules*, *12*(6), 2145–2152.

Manski, J. M., van der Goot, A. J., & Boom, R. M. (2007). Formation of fibrous materials from dense calcium caseinate dispersions. *Biomacromolecules*, *8*(4), 1271–1279.

Maranzano, B. J., & Wagner, N. J. (2002). Flow-small angle neutron scattering measurements of colloidal dispersion microstructure evolution through the shear thickening transition. *The Journal of Chemical Physics*, *117*(22), 10291–10302.

Matsunaga, T., Asai, H., Akagi, Y., Sakai, T., Chung, U.-i., & Shibayama, M. (2011). SANS studies on Tetra-PEG Gel under uniaxial deformation. *Macromolecules*, *44*(5), 1203–1210.

Maurya, A. K., Weidenbacher, L., Spano, F., Fortunato, G., Rossi, R. M., Frenz, M., et al. (2019). Structural insights into semicrystalline states of electrospun nanofibers: a multiscale analytical approach. *Nanoscale*, *11*(15), 7176–7187.

Miyazaki, S., Karino, T., Endo, H., Haraguchi, K., & Shibayama, M. (2006). Clay Concentration Dependence of Microstructure in Deformed Poly (N-isopropylacrylamide)-Clay Nanocomposite Gels. *Macromolecules*, *39*(23), 8112–8120.

Perret, R., & Ruland, W. (1969). Single and multiple X-ray small-angle scattering of carbon fibres. *Journal of Applied Crystallography*, *2*(5), 209–218.

Ratnaweera, D. R., Saha, D., Pingali, S. V., Labbé, N., Naskar, A. K., & Dadmun, M. (2015). The impact of lignin source on its self-assembly in solution. *RSC Advances*, *5*(82), 67258–67266.

Ruland, W. (1969). Small-angle scattering studies on carbonized cellulose fibers. *Journal of Polymer Science Part C: Polymer Symposia*, *28*(1), 143–151.

Schmidt, G., Nakatani, A. I., Butler, P. D., & Han, C. C. (2002). Small-angle neutron scattering from viscoelastic polymer- clay solutions. *Macromolecules*, *35*(12), 4725–4732.

Tian, B., Wang, Z., de Campo, L., Gilbert, E. P., Dalgliesh, R. M., Velichko, E., et al. (2020). Small angle neutron scattering quantifies the hierarchical structure in fibrous calcium caseinate. *Food Hydrocolloids*, *106*, Article 105912.

Vogtt, K., Beaucage, G., Weaver, M., & Jiang, H. (2015). Scattering function for branched wormlike chains. *Langmuir*, *31*(30), 8228–8234.

Wang, Z., Tian, B., Boom, R., & van der Goot, A. J. (2019). Air bubbles in calcium caseinate fibrous material enhances anisotropy. *Food Hydrocolloids*, *87*, 497–505.

Weigandt, K. M., Porcar, L., & Pozzo, D. C. (2011). In situ neutron scattering study of structural transitions in fibrin networks under shear deformation. *Soft Matter*, *7*(21), 9992–10000.

Won, Y.-Y., Davis, H. T., & Bates, F. S. (1999). Giant wormlike rubber micelles. *Science*, *283*(5404), 960–963.

Worcester, D., Michalski, T., & Katz, J. (1986). Small-angle neutron scattering studies of chlorophyll micelles: models for bacterial antenna chlorophyll. *Proceedings of the National Academy of Sciences*, *83*(11), 3791–3795.

Yang, H., Liu, D., Ju, J., Li, J., Wang, Z., Yan, G., et al. (2016). Chain deformation on the formation of shish nuclei under extension flow: an in situ SANS and SAXS study. *Macromolecules*, *49*(23), 9080–9088.

Yong, W., Lomakin, A., Kirkitadze, M. D., Teplow, D. B., Chen, S.-H., & Benedek, G. B. (2002). Structure determination of micelle-like intermediates in amyloid β-protein fibril assembly by using small angle neutron scattering. *Proceedings of the National Academy of Sciences*, *99*(1), 150–154.